Peroxidase biomimetic system based on Fe_3O_4 nanoparticles in non-enzymatic sensors

Juan A. Ramos Guivar, Edson G.R. Fernandes, Valtencir Zucolotto

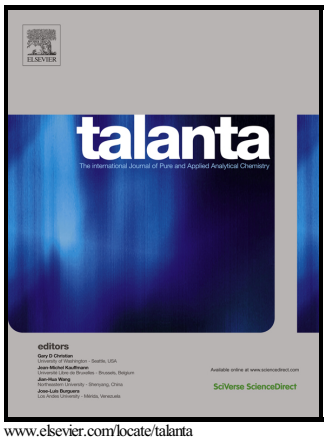

www.elsevier.com/locate/talanta

PII: S0039-9140(15)00170-8
DOI: http://dx.doi.org/10.1016/j.talanta.2015.03.017
Reference: TAL15450

To appear in: *Talanta*

Received date: 12 December 2014
Revised date: 9 March 2015
Accepted date: 11 March 2015

Cite this article as: Juan A. Ramos Guivar, Edson G.R. Fernandes and Valtencir Zucolotto, Peroxidase biomimetic system based on Fe_3O_4 nanoparticles in non-enzymatic sensors, *Talanta,* http://dx.doi.org/10.1016/j.talanta.2015.03.017

Peroxidase biomimetic system based on Fe_3O_4 nanoparticles in non-enzymatic sensors

Juan A. Ramos Guivar[1*], Edson G. R. Fernandes[2], Valtencir Zucolotto[2]

[1] Ceramics and Nanomaterials Laboratory, Facultad de Ciencias Físicas, Universidad Nacional Mayor de San Marcos, Ap. Postal 14-0149, Lima 14, Perú

[2] Nanomedicine and Nanotoxicology Laboratory, Instituto de Física de São Carlos, Universidade de São Paulo, CP 369, 13560-970 São Carlos, SP, Brazil

[*]Corresponding author: Juan A. Ramos Guivar, Ceramics and Nanomaterials Laboratory, Facultad de Ciencias Físicas, Universidad Nacional Mayor de San Marcos, Calle Germán Amézaga Nº375-Lima 01, Perú. Phone: (0051) (1) 940298993, e-mail: aguivar@gmail.com

Abstract

Novel and innovative applications of magnetic nanoparticles are being applied at many areas of nanomedicine. Sensing platforms based on this type of nanoparticles have received a lot of attention due to the relative low cost of producing, biocompatibility, environmentally safe, the intrinsic magnetic properties, etc. Biosensor is the most widely study type of analytical device. This type of sensor combines the physicochemical transduction with the incorporation of a biological sensing component. Among the biological components, enzymes are the most commonly used as sensitive element. But natural enzymes can present some serious disadvantages such as protein stability and loss of catalytic activity by immobilization method. Then, the study of enzymes biomimetic

systems are of great interest. This study reports the development of a new sensor composed of Fe_3O_4@CTAB and poly(sodium 4-styrenesulfonate) (PSS) film assembled via Layer-by-Layer (LbL) technique as peroxidase mimetic catalyst. Magnetic nanoparticles (MNps) were synthesized using thermal decomposition method and further lead to aqueous medium by ligand modification reaction using cetyltrimethylammonium bromide (CTAB). The amperometric detection limit of H_2O_2 was found to be ca. 103 μmol L^{-1} (this value results in 4.5 μmol L^{-1} for voltammetry analysis) at a signal-to-noise ratio of 3. By chronoamperometry, the peroxidase biomimetic sensor has a ~~good~~ linear relationship with H_2O_2 in the range from 100 μmol L^{-1} to 1.8 mmol L^{-1}. (R^2 = 0.994) with ~~good~~ sensitivity of 16 nA mol^{-1} L. The apparent Michaelis-Menten constant K_m^{app} was 5.3 mmol L^{-1}, comparable with some biosensors based on peroxidase enzyme. Moreover, the sensor had a reproducibility of ca. 7.7% (n = 4) and their response (response time: 90 s) is not significantly affected by some interferences: K^+, Na^+, Cl^-, Mg^{2+}, Ca^{2+}, and Uric Acid. The work potential is -0.3 V vs. Ag/AgCl electrode.

Keywords: Biomimetic sensor; Layer-by-Layer films; Magnetic nanoparticles; Hydrogen peroxide.

1. Introduction

Novel and innovative applications of magnetic nanoparticles (Fe_3O_4@, Fe_2O_3@) are being applied at many areas of nanomedicine such as drug delivery systems, contrast agent for magnetic resonance, hyperthermia for cancer treatment, biosensing, etc. [1]. Recently,

new sensors based on magnetic nanoparticles/polymer systems deposited on conductor tin doped indium oxide (ITO) and fluorine doped tin oxide (FTO) substrates are captured researchers attention. In a previous work of our research group [2], Marangoni et al. reported the functionalization of magnetite nanoparticles with the polyelectrolyte poly (diallyldimethylammonium chloride) (PDAC) immobilized onto ITO films by Layer-by-Layer (LbL) technique [3]. Fe_3O_4@PDAC onto ITO electrodes in acidic electrolyte displayed a redox couple attributed to Fe(II)/Fe(III), where the faradaic current increased in a linear form with the number of deposited bilayers denoting possible applications in nanoelectronics and bioelectrochemical devices. Martins et al. reported the synthesis of metastable phase of iron oxide and iron hydroxide nanoparticles (PDAC–FeOOH/Fe_2O_3@) to be used in biofuel cells [4]. In this study, we describe the deposition of magnetite nanoparticles stabilized with cetyltrimethylammonium bromide (Fe_3O_4@CTAB)/poly (sodium 4-styrenesulfonate) (PSS) onto FTO substrates using Layer-by-Layer technique. For that, Fe_3O_4@CTAB and PSS solutions were deposited on glass substrates and the film growth was monitored by UV-Vis spectroscopy. Then, the catalytic behavior of the LbL films trough H_2O_2 was performed by the electrochemical analyses of FTO-Fe_3O_4@CTAB/PSS 2-bilayers.

The determination of H_2O_2 is of great interest in environmental, food pharmaceutical and clinical analysis [5]. Several techniques such as fluorescence [6], spectrophotometry, titrimetric, and electrochemical techniques have been employed in the hydrogen peroxide detection [5-7]. Among these methods, electrochemical techniques have attracted a lot of interest due to their relative low response time, cost, size and simplicity [7].

Horseradish peroxide (HRP) is the most common enzyme used in biosensing devices for H_2O_2 detection due to their heme prosthetic group [7]. Other redox enzymes used for H_2O_2 detection are cytochrome-c and hemoglobin [7] -- all that cited enzymes possess an iron metal as catalytic agent in their prosthetic group. The principal problem with this type of sensors is the long-term stability of the proteins [8-9]. Another problem is the orientation of the active prosthetic group of the immobilized enzyme and the protein denaturation, which can decrease the direct electron transfer between the catalytic element and the electrode [9-10].

In the last years, nanoparticles have been used as catalytic element as enzyme substitute in various "enzymeless biosensors" [2, 4, 11]. For example, Mu et al. [12] propose the catalysis of the decomposition of H_2O_2 to oxygen using Co_3O_4 nanoparticles as a catalase mimic system. Gao et al. reported the catalytic activity of Fe_3O_4 nanoparticles as peroxidase mimetic to detect H_2O_2 and discus their potential applications in medicine, environmental chemistry and biotechnology [13]. Šljukić et al. reported that the catalytic activity of carbon nanotubes for H_2O_2 reduction is attributed to iron oxide impurities [14]. Liu et al. also developed Fe_3O_4-Ag hybrid sub-microspheres (estimated average diameter of 400 nm) for the electrochemical detection of H_2O_2 [15]. Yu et al. reported the fabrication of biosensors using Fe_3O_4 nanoparticles as a core in Pt core-shell structure (Fe_3O_4@Pt) assembled by LbL technique with hemoglobin for H_2O_2 and nitrite detection [16].

In this paper, we report on a novel sensor for determination of H_2O_2 based on the LbL assembling of Fe_3O_4@CTAB highly stable nanoparticles and PSS, with the aim of providing its use as peroxidases substitute in enzymeless biosensors for H_2O_2 detection. In this sense, we detect hydrogen peroxide by electrochemical technique (cyclic voltammetry

and chronoamperometry): the apparent Michaelis-Menten constant (K_m^{app}) is close to values found in enzyme-based biosensors (5.3 mmol L^{-1}).

2. Experimental

2.1. Materials

All chemicals reagents used in this experiment were of analytical grade and used without any further purification. $Fe(acac)_3$, KCl, NaCl, $MgCl_2$, $CaCl_2$, Uric Acid, Oleylamine, oleic acid, Cyclohexane, CTAB, KOH, KH_2PO_4, K_2HPO_4 and $K_3Fe(CN)_6$ were purchased from Sigma-Aldrich. Hydrogen peroxide (H_2O_2, 30%) and NaOH were purchased from Synth. The ultrapure water used for Fe_3O_4@CTAB synthesis, LbL films and electrochemical experiments were obtained from an ultrapure water system (Megapurity System®, resistivity of 18.3 MΩ cm). Commercial FTO covered glass (Sigma-Aldrich) was used due to their relative low cost and amphoteric surface. The FTO substrates were cleaned by sonication sequentially in: acetone, ethanol, isopropyl alcohol and NaOH solution during 10 minutes each one. Then, they were washed with deionized water and dried in a N_2 flow.

2.2. Synthesis of the Fe_3O_4 nanoparticles by thermal decomposition

The synthesis of magnetic nanoparticles was performed according to the thermal decomposition method proposed by Sun et al [17]. Briefly, 0.7 g of $Fe(acac)_3$ and 2.58 g of 1,2-hexadecanediol were dissolved in 20 mL of benzyl ether at 100 °C under N_2 atmosphere and magnetic stirring. After 30 minutes, 1.97 mL of oleylamine and 1.97 mL of oleic acid were added. The system was heated to reflux (about 300 °C) during two hours under vigorous stirring. Then, the heating source was turned off, and when the system was at room temperature (RT), 20 mL of absolute ethanol was added. The particles were magnetically

separated and wash one more time in ethanol. After all, the particles were magnetically separated and suspended in cyclohexane [18].

2.3. Synthesis of CTAB- modified Fe_3O_4 MNPs

For the synthesis, 9 ml of CTAB (0.1 mol L^{-1}) was mixtured with 2 mL of isopropanol with vigorous stirring, 700 µL of Fe_3O_4 nanoparticles suspended in cyclohexane was added. The system was kept for 3 hours at bath sonicator (vortex every 15 minutes to avoid phase separation). After that, the system was stirred at about 35 °C in opened flask until isopropanol and cyclohexane was completely evaporated turning into a hydrophilic state.

2.4. XRD and TEM Characterization

XRD data were obtained at the Laboratory of X-ray Crystallography of IFSC/USP using a Rigaku Rotaflex diffractometer equipped with graphite monochromator and rotating anode tube, operating with CuKα radiation (1.5406 Å), 50 kV and 100 mA. Powder diffraction patterns were obtained in step scanning mode, 2θ = 27 - 77°, step of 0.01° and 4 seconds/step.

The morphology and particle size were analyzed by transmission electron microscopy (TEM) JEOL/JEM-2100 at the acceleration voltage of 200 kV. The samples were prepared by deposition of one drop of the diluted samples on a carbon film copper grid 300 mesh (Ted Pella, Inc.). The average diameter for the particles coated at first with OAM/OA and then with CTAB was evaluated using ImageJ software from the US National Institute of Health.

2.5. LbL films

The pK_a of the PSS is about 1.0 and the synthesized Fe_3O_4 nanoparticles are positive charged at pH 7.0. The Zeta potential (ζ) values of the solution used for LbL was carried out using Zeta sizer (Malvern Zs 90, U.K.). The LbL films were made by LbL self-assembling through the alternating deposition of Fe_3O_4 nanoparticles (Fe_3O_4@CTAB) and poly(sodium 4-styrenesulfonate) (PSS): firstly, the FTO substrates were immersed in a Fe_3O_4@CTAB solution (pH 12) for 5 min, then, rinsed in a NaOH solution (pH 12) for few seconds and gently dried in a N_2 flux. After, the second layer was formed by the immersion of the substrate in a PSS solution (water, 1 g L^{-1}, pH 7) for 3 min, and then rinsed in a water solution and dried in a N_2 flux. The process was repeated one more time to get the first 2-bilayer, and subsequently 4, 5, 6, 8 and 10-bilayer. The film growth was monitored by electronic absorption using an UV–Vis spectroscopy (Hitachi U-2900, China). FTIR (Thermo Scientific Nicolet iS50, U.S.A.) measurements were carried out in the transmission mode for Fe_3O_4@CTAB casting, PSS casting, Fe_3O_4@CTAB + PSS casting and $[Fe_3O_4@CTAB/PSS]_{15}$ LbL film. FTIR was performed by using a resolution of 4 cm^{-1}. The cast films were produced by dropping ca. 10 µL onto Silicon wafer (111) and dried in an oven at 60°C for 60 minutes. The same type Silicon wafer (111) was used to LbL film growth. AFM measurements were carried out using a Shimadzu scanning probe microscope (SPM-9600). Tapping mode was used for sample surface topography.

2.6. Electrochemical measurements

The electrochemistry was carried out in a potentiostat/galvanostat (Autolab, Princeton, U.K.) using a conventional three-electrode cell. The LbL Fe_3O_4@/PSS films were used as working electrodes. The reference electrode was Ag/AgCl/KCl 3M and the counter electrode was a platinum plate (0.5 cm x 1 cm). Cyclic voltammograms were

registered from –1.0 to +1.0 V at a sweep rate of 50 mV s^{-1} (except when indicated otherwise). Phosphate buffer solution (PB, 0.1 mol L^{-1}, pH 7.2) and KCl (0.1 mol L^{-1}) was used as supporting electrolyte with a volume cell of 10 mL. Chronoamperometry measurements were performed under an applied potential of -0.3 V (vs. Ag/AgCl) by successive addition of H_2O_2 100 μmol L^{-1}. After each addition of H_2O_2, the cell solution was stirred (about one minute) using a magnetic stirrer and the measurements were performed in static condition. Before each experiment, all standard solution of hydrogen peroxide was freshly prepared. The interferences measurement was made under stirring solution.

3. Results and discussions

XRD powder diffraction pattern is shown in Fig. 1a. It reveals only one phase associated to spinel cubic structure of magnetite (Fe_3O_4). Miller planes have been indexed using JCPDS file 19-0629. The broadened peaks are associated to nanoscopic size of the MNPs. X-ray diffraction technique examines the long-range order produced as a consequence of very short-range interactions. Powder diffractogram of Fe_3O_4 nanoparticles in Fig. 1a exhibited broad peaks at 2θ = 30.6; 35.9; 43.4; 53.8; 57.3; 62.7; 71.2 and 74.8 °. The inset of Fig. 1a shows the attraction of the superparamagnetic nanoparticles when an external constant magnetic field was applied.

TEM pictures (Fig. 1b and c) shows the morphology of the magnetic nanoparticles with monodispersity and narrow size distribution often obtained by thermal decomposition route [17]. Homogeneous spherical morphology of Fe_3O_4@OAM-OA nanoparticles is regarded without present agglomeration and confirming high stability in organic medium

with mean diameter of (4.8 ± 0.6) nm (polidispersity = 13 %, see inset in Fig. 1a). The image in Fig. 1b depicts nanoparticles stabilized with CTAB in aqueous medium, showing the nanoparticles embedded in a matrix of CTAB with mean diameter of (4.7 ± 0.8) nm with polidispersity value of 17 % (see the inset in Fig. 1b).

Please, Figure 1 here

Film growth was monitored by measuring the absorption band at 390 nm, attributed to the formation of the Fe_3O_4@CTAB/PSS complex, upon deposition of successive bilayers (we assume that the linear growth (R^2 = 0.975) indicates the deposition of the same adsorbed amount of material for each bilayer deposition). LbL deposition of the Fe_3O_4@CTAB/PSS solution on the surface of the glass substrate shows good reproducibility as one can see at Fig. 2 (each point corresponds to the average of three different substrates). The UV–Vis spectroscopy of the LbL films is due to Fe_3O_4@CTAB which presents a broad absorption tail (characteristic of indirect band gap semiconductors), without any plasmonic band in the UV-Vis range [19]. Then, the increase of the absorption spectra with the increase of the number of bilayers is due to scattering effects. The LbL assembling of the films can be explained by Zeta Potential (ZP) of the chemical species in the immersion solutions (three measurements): a) ZP for PSS in pH 7 solution was –(64.6 ± 4.5) mV; b) ZP for PSS in NaOH solution (pH 12) was –(44 ± 4) mV; c) Fe_3O_4@CTAB in pH 7 solution was +(90.4 ± 4.5) mV; and d) Fe_3O_4@CTAB in pH 12 solution was +(76 ± 4) mV. Marangoni et al. reported a zeta potential of +68 mV for a suspension of magnetic nanoparticles stabilized by poly (diallyldimethylammonium chloride) (Fe_3O_4@PDAC) at pH 10 [2]. Then, the LbL films of Fe_3O_4@CTAB/PSS were deposited on FTO substrates (negative charge surface) by the alternate immersion of the substrates on nanoparticles

suspension and PSS solution, respectively. Dey et al. reported an enhancement in the electrostatic assembly of magnetic nanoparticles applying a magnetic field (300 mT) perpendicular to the substrates [20].

Please, Figure 2 here

Figure 3 shows Fourier transform spectroscopy (FTIR) spectra of pure Fe_3O_4@CTAB, PSS, Fe_3O_4@CTAB + PSS solution and Fe_3O_4@CTAB/PSS films grown on Si-wafer (111) and their frequencies are listed with their possible assignments: in the spectral region 3550–2500 cm^{-1}, the C–H symmetric and asymmetric stretching vibration frequency modes at 2849 and 2919 cm^{-1} are assigned to pure CTAB. The doublet at 1462 and 1472 cm^{-1} for pure CTAB may be attributed to the CH_2–scissoring modes of vibrations. The characteristic bands associated to alkyl tails of CTAB appeared as symmetric bounds CH_3 at 1395 cm^{-1}. The vibrations of the bounds CH_3^+ in the symmetric plane with bound CH_2 is observed at 1465 cm^{-1}, the symmetric and asymmetric vibrations for CH_2 are showed at 2845 y 2922 cm^{-1}, respectively. It is worth mentioning that these bands are a superposition of $\nu_s CH_2$ and $\nu_{as} CH_2$ corresponding to OAM/OA and CTAB and cause a decrease in the intensity comparing to pure CTAB. In addition asymmetric vibration corresponding to $N(CH_3)_3^+$ is regarded at 3015 cm^{-1}. For C-N stretching modes of vibration the bands at around 960 and 1034 cm^{-1} are also observed. The characteristic absorption bands of the hydrophobic Fe_3O_4 nanoparticles at 630, 588 and 442 cm^{-1} are attributed to Fe–O bonds. Especially, the band at 588 cm^{-1} refers to Fe-O deformation in octahedral and tetrahedral sites in the inverse spinel cubic structure of magnetite [21]. For PSS spectrum, the vibrational bands are given: 1. 3700 - 3000 cm^{-1}: stretching vibration of hydroxyl functional groups; 2. 3100 cm^{-1} (three peaks): aromatic =C-H stretching vibrations; 3. 2920

cm^{-1} (two peaks): alkyl C-H stretching vibrations; 4. 1810 and 1925 cm^{-1}: aromatic C-H out of plane bending vibrations; 5. 1640 cm^{-1}: O-H bending vibrations of H_2O; 6. 1600, 1500, 1450 and 1410 cm^{-1}: aromatic -C=C- stretching vibrations; 7. 1190 and 1130 cm^{-1}: $-SO^{3-}$ asymmetric stretching vibrations; 8. 1040 and 1005 cm^{-1}: $-SO^{3-}$ symmetric stretching vibrations; 9. 836, 771 and 682 cm^{-1}: =C-H out of plane deformation vibrations; 10. 620 cm^{-1}: ring in-plane deformation vibrations. It can be seen that Fe_3O_4@CTAB and PSS described strong and middle intensity. However, intensity decreases for Fe_3O_4@CTAB/PSS films probably as a consequence of some chemical process carried out on the films and described later in this work (also see Table S1 and S2 in Supplementary data).

Please, Figure 3 here

Morphological aspects on the surface of the multilayer system were performed with AFM measurements. Figure 4 shows that the self-assembled nanoparticles preserved their spherical shape but forming aggregates with uniform diameter of 50 nm, approximately. It is worthy to mention that these aggregates can be formed due to the polymer present in the substrate. Figure 4a reveals the three-dimensional aspects of the large number of granular Fe_3O_4@CTAB/PSS particles covered the glass surface for 2-bilayers. After increasing the number of bilayers up to 10 bilayers a decrease on the high of the roughness values is observed (Fig. 4b). Additionally, Table I summarizes the roughness average (R_a) and root mean square roughness (R_q) values for the number of bilayers deposited on glass substrate.

Please, Figure 4 here

The roughness average, R_a, is calculated as follows:

$$R_a = \sum_{j=1}^{N} \frac{\left|Z_j - Z^*\right|}{N}$$

And the Root Mean Square roughness, R_q, is:

$$R_q = \sqrt{\sum_{j=1}^{N} \frac{\left|Z_j - Z^*\right|^2}{N-1}}$$

Where Z_j is the individual height value of the j-th measured point, Z^* is the mean value of all height points and N is the number of measurement points.

The sensing properties of 2-bilayer LbL films of Fe_3O_4@CTAB/PSS were tested towards PB solution (phosphate buffer at 0.1 mol L^{-1}, pH 7.2) and after H_2O_2 addition (500 μmol L^{-1}) at 50 mV s^{-1}, in a purged and non-purged N_2 solution. By the voltammograms, it is evident that the LbL films show response to hydrogen peroxide which is more evident in no-purging solution (Fig. 5). The inset of Fig. 5 shows the catalytic activity of the Fe_3O_4@CTAB/PSS: as one can see it is noticeable the shift of the cathodic potential for H_2O_2 reduction from -0.67 V (bare FTO electrode) to -0.48 V (Fe_3O_4@CTAB/PSS 2-bilayer film). The increase in the VC response in electrolytic solution without N_2 purging is due to the possible catalytic reduction of oxygen at the substrate [22].

Then, the subsequent measurements of H_2O_2 detection were made purging the electrolyte solution with N_2. The reduction potential for H_2O_2 onto Fe_3O_4@CTAB/PSS substrates is about -0.5 V. Figure 6 shows that the cathodic peak current increases with increasing the H_2O_2 concentration, and the electrocatalytic activity of the LbL film toward hydrogen peroxide reduction (in purged solution). The inset of Fig. 6 shows the analytical curve of

the LbL 2-bilayer film after successively H_2O_2 addition. The sensor has a good linear relationship with H_2O_2 in the range from 100 μmol L^{-1} to 1.8 mmol L^{-1} (R^2 = 0.994).

Please, Figure 5 here

Please, Figure 6 here

The pH solution adopted for the electrolyte solution (PB, pH 7.2) was based on the most common pH adopted for electrochemical detection of H_2O_2 [23]. Then, in this study we cannot infer a Fenton mechanism because the neutral electrolyte solution [24]. In Fenton reaction H_2O_2 is catalyzed by Fe(II)/Fe(III) ions in solution resulting in highly reactive radicals [25, 26]:

$$Fe(III)_{(surf)} + H_2O_2 \rightarrow Fe(II)_{(surf)} + OOH^{\bullet} + H^+$$

Whereas the reaction could be dominated by two stages in the electrode: 1) adsorption of the chemical species in the electrode and 2) surface catalyzed process (Scheme 1):

$$Fe_3O_4 + H_2O_2 \rightarrow (Fe_3O_4)H_2O_2$$

$$Fe(III)_{(surf)}(H_2O_2) + e^- \rightarrow Fe(II)_{(surf)} + HOO^{\bullet} + H^+$$

$$Fe(II)_{(surf)} + HOO^{\bullet} + H^+ \rightarrow Fe(III)_{(surf)} + H_2O + \frac{1}{2}O_2$$

The LbL Fe_3O_4@CTAB/PSS films are stable and the dissolution of Fe_3O_4 to FeO as reported by Hui et al. [27] do not occurs because of the low diffusion coefficient: estimated average value of 8.5 x 10^{-11} m^2 s^{-1} by Stokes-Einstein relation:

$$D = \frac{k_B T}{3\pi\eta\emptyset}$$

Where k_B is the Boltzmann constant (1.3806×10^{-23} J K^{-1}), T is the temperature (296 K), η is the viscosity of water (0.938 x 10^{-3} kg m^{-1} s^{-1} at 296 K) and ∅ is the average diameter of the nanoparticles (5 nm).

Martins et al. reported an average diffusion coefficient of 0.9 x 10^{-11} m^2 s^{-1} for PDAC–FeOOH/Fe_2O_3@ with average diameter of 20 nm [4]. The diffusion coefficient obtained in this study is almost ten times greater for an average diameter of 5 nm. But Fe_3O_4 is more stable than Fe_2O_3 and Fe^{3+} is not soluble in phosphate buffer such as Fe^{2+} which form a white precipitate ($FePO_4$) at pH 7 [28] (in both case, here and in Martins et al. study, the hydrodynamic radius was not taken into account).

The effective surface areas of the same size electrodes (limited by epoxy) was determined by cyclic voltammograms (CV) of 1.0 mmol L^{-1} of $K_3[Fe(CN)_6]$ as probe molecule in 0.1 mol L^{-1} of KCl solution, at different scan rates. Then, kinetic studies were carried out by registering the CV of the LbL films at scan rates from 0.015 to 0.400 V s^{-1} (temperature: (22 ± 2) °C).

Figure S1 (Supplementary data) shows the CV response of 2-bilayer LbL film at different scan rates. The peak at ca. 0.320 V and 0.210 V (50 mV s^{-1}) are associated to the oxidation and reduction of $[Fe(CN)_6]^{3-}$/$[Fe(CN)_6]^{4-}$ pair. Figure S1 also shows an anodic peak shift to positive potentials and a shift of the cathodic peak to negative ones, with the increase of the scan rate. The relation of the anodic and cathodic peak response is $I_{pa}/I_{pc} =$ 0.85 ± 0.06, different from the theoretical value of 1 for reversible systems. Then, the

charge transfer on the electrode is almost nernstian in a quasi-reversible electrocatalytical process. In addition, the response current increases in a linear relationship with the square root of scan rates in the range of 10–400 mV s^{-1} (R^2: 0.996), indicating a diffusion-controlled process and confirm the assumption above. These results are in agreement with a similar system proposed by Martins et al. in acid electrolyte solution (H_2SO_4, 0.1 mol L^{-1}) [4]. Therefore, the electron transfer kinetics is dominated by mass transport mechanism and indicates high ability of the film to promote electron transfer between the nanoparticles and the substrate [29].

The Randles-Ševičk method [30-32] was used for the determination of the effective area, A, of the electrodes, according to the equation:

$$I_P = (2.687 \times 10^5) n^{3/2} A D^{1/2} \nu^{1/2} C$$

Where I_p is the peak current, A is the electrode surface area (cm^2), D is the diffusion coefficient (cm^2 s^{-1}), and C is the bulk concentration of $K_3[Fe(CN)_6]$ (mol cm^{-3}), n is the electron transfer number, F is the Faraday constant (96,485 C mol^{-1}), R is the universal gas constant (8,314 J K^{-1} mol^{-1}), T is temperature (298 K) and ν is the scan rate (V s^{-1}).

The effective surface area of the electrodes can be calculated from the slope of the I_p vs. $\nu^{1/2}$ plot (assuming the diffusion coefficient to the $[Fe(CN)_6]^{3-}$ of 7.60 x 10^{-6} cm^2 s^{-1} in KCl 0.1 mol L^{-1}) [33]. The values of A for different electrodes were determined as: for the 2-bilayer film, the effective electrode surface was 0.0127 cm^2 whereas for 5-bilayer film was 0.0124 cm^2 (virtually the same area) and for 10-bilayer film the area decreased to 0.0114 cm^2. The results are in agreement with the decrease of surface rough calculated by AFM analysis (Table I).

The same kinetic study was made for H_2O_2 catalysis and the results confirm that the reaction was diffusion controlled in the scan range studied (5 – 500 mV s^{-1}) (Fig. 7). The diffusion coefficient for H_2O_2 was estimated using the Randles-Ševičk equation for 2-bilayer LbL film of Fe_3O_4@CTAB/PSS. The diffusion coefficient of H_2O_2 was calculated to be about 2.6 x $10^{-6}$$cm^2$ s^{-1} (assuming a 2-electron reaction: n = 2 suggesting a reversible electron transfer trough the electrode (magnetic nanoparticles redox) for the first transferring electron followed by an irreversible step due to the hydrogen peroxide catalysis and/or lateral interactions of the redox couple present in the film). The D value obtained was almost identical to reported value for other biomimetic systems. For example, Guascito et al. reported a value of 1.0 x 10^{-5} cm^2 s^{-1} for the diffusion coefficient to H_2O_2 in film of polyvinyl alcohol (PVA) containing immobilized silver nanoparticles on a platinum electrode [34]. In addition, applying the calculated diffusion coefficient value of H_2O_2 in the Stokes-Einstein relation, the H_2O_2 hydrodynamic radius may be estimated in 1 x 10^{-10} m. This value is confirmed considering molecular dynamics simulations (average value of 2.4 x 10^{-10} m) as reported by Fogolari et al. [35].

Please, Figure 7 here

The best applied potential on the determination of H_2O_2 by chronoamperometry was also investigated (Fig. S2). To confirm the best-applied work potential for the 2-bilayer LbL film ([Fe_3O_4@CTAB/PSS]$_2$), the response current was recorded as a function of the applied potential in presence of 1.4 mmol L^{-1} of H_2O_2. The cathodic current reached a maximum value at around -0.5 V (this value is confirmed by the CV curves), after which the response current remained practically constant at value of ca. 35 μA. About 75% of the

response current is achieved at the chosen potential of -0.3 V. The sensor reached a stead state, 95% of the maximum response signal, within 60 s.

Figure 8 presented the chronoamperometric results for successive addition of H_2O_2, at the applied work potential of -0.3 V vs. Ag/AgCl in PB (0.1 mol L^{-1}, pH 7.2). The analytical plot is the average of three distinct electrodes (the inset of the Fig. 8). The linear range for H_2O_2 is 100 μmol L^{-1} – 1.6 mmol L^{-1} (R^2: 0.992). The analytical plot is the average of three distinct electrodes (response time of 60 s). The limit of detection (LOD) for H_2O_2 was calculated according with the $3\sigma/b$ criterion, where σ is the standard deviation (n = 7) of the blank (-3,35 ± 0,55 μA, PB, 0.1 mol L^{-1} at pH 7.2) and b is the analytical curve slope. The LOD was estimated at 103 μmol L^{-1} (this value results in 4.5 μmol L^{-1} for VC analysis: blank current of -10,34 ± 014 μA). The sensitivity of $[Fe_3O_4@CTAB/PSS]_2$ for hydrogen peroxide is 16 nA μmol^{-1} L (angular coefficient of the I_p vs. $[H_2O_2]$) (the obtained sensitivity by VC was 94 nA μmol^{-1} L).

Please, Figure 8 here

The amperometric response is highly reproducible with a standard deviation (n = 4) of ca. 7.7%, similar to what has been reported in literature.

The reusability of the sensor was also investigated by collected successive amperometric response and the sensors could be used for 3 measurements with a decrease of ca. 10% in the signal (after the first measurement). The LbL film reproducibility was examined for three sensors units resulting in a relative standard deviation (R.S.D.) of 6.4 % for 100 μmol L^{-1} of H_2O_2, 7.8% for 400 μmol L^{-1} of H_2O_2, and 2.8% for 1.6 mmol L^{-1} of H_2O_2.

Please, Figure 9 here

Six species were studied by chronoamperometry in hydrodynamic conditions to evaluate the interference in the H_2O_2 catalysis: K^+, Na^+, Cl^-, Mg^{2+}, Ca^{2+}, and Uric Acid (as one can see in Fig. 9). The result suggested that the studied species had no obvious interference in the H_2O_2 reduction. He et al. reported the recovered of ca. 100% of H_2O_2 in the presence of: Na^+, K^+, NH_4^+, Ca^{2+}, Mg^{2+}, Zn^{2+}, Pb^{2+}, Al^{3+}, Ni^{2+}, $Cr^{3+}$and Co^{2+} as interferences [36].

In order to compare this study with other biomimetic systems, the Lineweaver-Burk plot (Fig. S3) was construct and the apparent Michaelis-Menten constant (K_m^{app}) was calculated according to the equation [37]:

$$\frac{1}{I_{Sat}} = \frac{1}{I_{max}} + \frac{K_m^{app}}{I_{max}} \frac{1}{[H_2O_2]}$$

Where I_{Sat} is the steady-state current after the addition of H_2O_2, $I_{max}$is the maximum current measured under saturation condition and $[H_2O_2]$ is the bulk concentration of H_2O_2.

The K_m^{app} constant was calculated to be 5.3 mmol L^{-1}. This value is close to 4.6 mmol L^{-1} and 4.51 mmol L^{-1} for biosensor based on HRP enzyme in a sol–gel/hydrogel composite film and HRP immobilized into a matrix of ormosil modified with multiwalled carbon nanotubes and nile blue as mediator agent, respectively [38, 39]. In addition, the value of 5.3 mmol L^{-1} is smaller than those 7.6 mmol L^{-1} for another biosensor based on HRP [40], 54.3 mmol L^{-1} for catalase and 34.7 mmol L^{-1} for Co_3O_4 nanoparticles as catalase mimic [12].

It is worthwhile to mention that the biomimetic system proposed here presents better characteristics in some cases and is comparable with some biosensors as can be seen in Table II.

Conclusions

A novel sensing platform based on Fe_3O_4 nanoparticles as peroxidase mimic system in LbL films was fabricated for determination of H_2O_2. CTAB stabilized Fe_3O_4 nanoparticles were firstly synthesized revealing good monodispersity with narrow size distribution according to TEM measurements (diameter of 4.8 ± 0.6 nm, index of polidispersity: 13 %,). The solution stability of the magnetic nanoparticles stabilized with CTAB was confirmed by Zeta potential (+ (90.4 ± 4.5) mV) at neutral pH. The interference tests (K^+, Na^+, Cl^-, Mg^{2+}, Ca^{2+}, and Uric Acid) confirmed that the sensor presents some selective to H_2O_2 and is comparable with some enzyme based biosensors (K_m^{app} of 5.3 mmol L^{-1}). The resulting enzymeless biosensor exhibited a good analytical performance in the range of 100 μmol L^{-1} from 1.8 mmol L^{-1} of H_2O_2. By chronoamperometry, the sensor showed limit of detection about 103 μmol L^{-1}, good sensitivity of 16 nA μmol^{-1} L and reproducibility (ca. 7.7%, n = 4). The work potential was -0.3 V vs. Ag/AgCl electrode. It is worthwhile to mention that the LbL Fe_3O_4@CTAB/PSS film proposed here presents better characteristics in some cases and is comparable with some biosensors (K_m^{app} constant of 5.3 mmol L^{-1}). In addition, the present study can be extended for the development of enzyme-based biosensors which can produce H_2O_2 in their catalysis.

Acknowledgments

The authors are grateful to the CAPES (project PNPD20131739) for the financial support. We also wish to thank José Augusto Lopes da Rocha, Lab Technician of the IFSC/USP, for their assistance in the X-Ray Diffractometer.

References

[1] A. Ito, M. Shinkai, H. Honda, T. Kobayashi, Medical application of functionalized magnetic nanoparticles, J. Biosci. Bioeng. 100 (2005) 1-11.

[2] V. S. Marangoni, M. V. A. Martins, J. A. Souza, O. N. Oliveira Jr., V. Zucolotto, F. N. Crespilho, The processing of polyelectrolyte-covered magnetite nanoparticles in the form of nanostructured thin films, J. Nanopart. Res. 14 (2012) 769.

[3] D. Gero, Fuzzy nanoassemblies: toward layered polymeric multicomposites, Science 277 (5330) 1232–1237.

[4] M. V. A. Martins, C. Bonfim, W. C. da Silva, F. N. Crespilho, Iron (III) nanocomposites for enzyme-less biomimetic cathode: A promising material for use in biofuel cells, Electrochem. Commun. 12 (2010) 1509–1512.

[5] M. Tarvin, B. McCord, K. Mount, K. Sherlachd, M. L. Miller, Optimization of two methods for the analysis of hydrogen peroxide: High performance liquid chromatography with fluorescence detection and high performance liquid chromatography with

electrochemical detection in direct current mode, J. Chromatogr. A 1217 (2010) 7564–7572.

[6] H. Jin, D. A. Heller, M. Kalbacova, Jong-Ho Kim, J. Zhang, A. A. Boghossian, N. Maheshri & M. S. Strano, Detection of single-molecule H_2O_2 signalling from epidermal growth factor receptor using fluorescent single-walled carbon nanotubes, Nat. Nanotechnol. 5 (2010) 302 – 309.

[7] W. Chen, S. Cai, Q. Q. Ren, W. Wen and Y. D. Zhao, Recent advances in electrochemical sensing for hydrogen peroxide: a review, Analyst 137 (2012), 49–58.

[8] S.J. Guo, S.J. Dong, E.K. Wang, Polyaniline/Pt Hybrid Nanofibers: High-Efficiency Nanoelectrocatalysts for Electrochemical Devices, Small 5 (2009) 1869–1876.

[9] M.D. Gouda, M.A. Kumar, M.S. Thakur, N.G. Karanth, Enhancement of operational stability of an enzyme biosensor for glucose and sucrose using protein based stabilizing agents, Biosens. Bioelectron. 17 (2002) 503-507.

[10] E. G. R. Fernandes, L. C. Brazaca, M. L. Rodríguez-Mendez, J. A. de Saja, V. Zucolotto, Immobilization of lutetium bisphthalocyanine in nanostructured biomimetic sensors using the LbL technique for phenol detection, Biosens. Bioelectron. 26 (2011) 4715– 4719.

[11] H. Wei and E. Wang, Fe_3O_4 Magnetic Nanoparticles as Peroxidase Mimetics and Their Applications in H_2O_2 and Glucose Detection, Anal. Chem. 80 (2008) 2250-2254.

[12] J. Mu, L. Zhang, M. Zhao, Y. Wang, Co_3O_4 nanoparticles as an efficient catalase mimic: Properties, mechanism and its electrocatalytic sensing application for hydrogen peroxide, J. Mol. Catal. A: Chemical 378 (2013) 30– 37.

[13] L.Z. Gao, J. Zhuang, L. Nie, J.B. Zhang, Y. Zhang, N. Gu, T.H. Wang, J. Feng, D.L. Yang, S. Perrett, X. Yan, Intrinsic peroxidase-like activity of ferromagnetic nanoparticles, Nat. Nanotechnol. 2 (2007) 577–583.

[14] B Šljukić, CE Banks, RG Compton, Iron oxide particles are the active sites for hydrogen peroxide sensing at multiwalled carbon nanotube modified electrodes, Nano Letters 6 (2006) 1556-1558.

[15] Z. Liu, B. Zhao, Y. Shi, C. Guo, H. Yang, Z. Li., Novel nonenzymatic hydrogen peroxide sensor based on iron oxide–silver hybrid submicrospheres, Talanta 81 (2010) 1650–1654.

[16] C. Yu, Y. Wang, L. Wang, Z. Zhu, N. Bao, H. Gu, Nanostructured biosensors built with layer-by-layer electrostatic assembly of hemoglobin and Fe_3O_4@Pt nanoparticles, Colloids Surf. B: Biointerfaces 103 (2013) 231– 237.

[17] S. Sun, H. Zeng, D. B. Robinson, S. Raoux, P. M. Rice, S. X. Wang and G. Li, Monodisperse MFe_2O_4 (M =Fe, Co, Mn) Nanoparticles, J. Am. Chem. Soc. 126 (2004) 273-279.

[18] J. Park, K. An, Y. Hwang, J. G. Park, H. J. Noh, J. Y. Kim, J. H. Park, N. M. Hwang and T. Hyeon, Ultra-large-scale syntheses of monodisperse nanocrystals, Nat. Mater. 3 (2004) 891-895.

[19] T.T. Baby, S. Ramaprabhu, SiO_2 coated Fe_3O_4 magnetic nanoparticle dispersed multiwalled carbon nanotubes based amperometric glucose biosensor, Talanta 80 (2010) 2016–2022.

[20] S. Dey, K. Mohanta, and A. J. Pal, Magnetic-Field-Assisted Layer-by-Layer Electrostatic Assembly of Ferromagnetic Nanoparticles, Langmuir 26 (2010) 9627–9631.

[21] Z. Xu, C. Shen, Y. Hou, H. Gao, and S. Sun, Oleylamine as Both Reducing Agent and Stabilizer in a Facile Synthesis of Magnetite Nanoparticles, Chem. Mater. 21 (2009) 1778–1780.

[22] A. J. Wang, Y. F. Li, Z. H. Li, J. J. Feng, Y. L. Sun, and J. R. Chen, Amperometric glucose sensor based on enhanced catalytic reduction of oxygen using glucose oxidase adsorbed onto core-shell Fe3O4@silica@Au magnetic nanoparticles, Mater. Sci. Eng. C 32 (2012) 1640–1647.

[23] M. Baghayeri, E. N. Zare, M. M. Lakouraj, A simple hydrogen peroxide biosensor based on a novel electro-magnetic poly(p-phenylenediamine)@Fe_3O_4nanocomposite, Biosens. Bioelectron. 55 (2014) 259–265.

[24] L. Xu, J. Wang, Fenton-like degradation of 2,4-dichlorophenol using Fe_3O_4 magnetic nanoparticles, Appl. Catal., B: Environ. 123 (2012) 117– 126.

[25] S., Goldstein, D. Meyerstein, G. Czapski. The Fenton reagents, Free radical biology and medicine 15(4) (1993) 435– 445.

[26] K. Rusevova, F.-D. Kopinke, A. Georgi. Nano-sized magnetic iron oxides as catalysts for heterogeneous Fenton-like reactions—Influence of Fe(II)/Fe(III) ratio on catalytic performance, J. Hazard. Mater. 241–242 (2012) 433–440.

[27] C. Hui, C. Shen, T. Yang, L. Bao, J. Tian, H. Ding, C. Li, and H. J. Gao, Large-Scale Fe_3O_4 Nanoparticles Soluble in Water Synthesized by a Facile Method, J. Phys. Chem. C 112 (2008) 11336–11339.

[28] F. Marken, D. Patel, C. E. Madden, R. C. Millward and S. Fletcher, The direct electrochemistry of ferritin compared with the directelectrochemistry of nanoparticulate hydrous ferric oxide, New J. Chem. 26 (2002) 259–263.

[29] J. Wang, Analytical Electrochemistry, second ed., Wiley-VCH, New York, 2001.

[30] J. E. B. Randles, A cathode ray polarograph. Part II. The current-voltage curves, Trans. Faraday Soc., 44 (1948) 327– 338.

[31] A. Ševičk, Oscillographic polarography with periodical triangular voltage, Collect. Czech. Chem. Commun. 13 (1948) 349-377.

[32] C. Apetrei, P. Alessio, C.J.L. Constantino, J.A. de Saja, M.L. Rodriguez-Mendez, F.J. Pavinatto, E. G. R. Fernandes, V. Zucolotto, O.N. Oliveira Jr., Biomimetic biosensor based on lipidic layers containing tyrosinase and lutetium bisphthalocyanine for the detection of antioxidants, Biosens. Bioelectron. 26 (2011) 2513–2519.

[33] R. Adams (1969) Electrochemistry at Solid Electrodes. Marcel Dekker, New York.

[34] M.R. Guascito, E. Filippo, C. Malitesta, D. Manno, A. Serra, A. Turco, A new amperometric nanostructured sensor for the analytical determination of hydrogen peroxide, Biosens. Bioelectron. 24 (2008) 1057–1063.

[35] F. Fogolari, A. Corazza, S. Toppo, S. C. E. Tosatto, P. Viglino, F. U. G. Esposito, Studying interactions by molecular dynamics simulations at high concentration, Journal of Biomedicine and Biotechnology. (2012) 1-9.

[36] S. He, W. Shia, X. Zhang, J. Li, Y. Huang, β-cyclodextrins-based inclusion complexes of $CoFe_2O_4$ magnetic nanoparticles as catalyst for the luminal chemiluminescence system and their applications in hydrogen peroxide detection, Talanta 82 (2010) 377–383.

[37] H. Bisswanger, in Enzyme Kinetics. Principles and Methods Ed. Wiley-VCH, T€ubingen, 2nd edn, 2008, ch. 2, pp. 66–77.

[38] B. Wang, J. Zhang, G. Cheng, S. Dong, Amperometric enzyme electrode for the determination of hydrogen peroxide based on sol–gel/hydrogel composite film, Anal. Chim. Acta 407 (2000) 111–118.

[39] T. Tangkuaram, C. Ponchio, T. Kangkasomboon, P. Katikawong, W. Veerasai, Design and development of a highly stable hydrogen peroxide biosensor on screen printed carbon electrode based on horseradish peroxidase bound with gold nanoparticles in the matrix of chitosan, Biosens. Bioelectron. 22 (2007) 2071–2078.

[40] M. Delvaux, A. Walcarius, S. D. Champagne, Electrocatalytic H_2O_2 amperometric detection using gold nanotube electrode ensembles, Anal. Chim. Acta 525 (2004) 221–230.

[41] Y. Xin, X. Fu-bing, L. Hong-wei, W. Feng, C. Di-zhao, W. Zhao, A novel H_2O_2 biosensor based on Fe_3O_4–Au magnetic nanoparticles coated horseradish peroxidase and graphene sheets–Nafion film modified screen-printed carbon electrode, Electrochim. Acta 109 (2013) 750– 755.

[42] X. C. Tan, J. L. Zhang, S. W. Tan, D. D. Zhao, Z. W. Huang, Y. Mi and Z. Y. Huang, Amperometric Hydrogen Peroxide Biosensor Based on Immobilization of Hemoglobin on a Glassy Carbon Electrode Modified with Fe_3O_4/Chitosan Core-Shell Microspheres, Sensors 9 (2009) 6185-6199.

[43] D. Baratella, M. Magro, G. Sinigaglia, R. Zboril, G. Salviulo, F. Vianello, A glucose biosensor based on surface active maghemite nanoparticles, Biosens. Bioelectron. 45 (2013) 13–18.

Figure and Table captions

Fig. 1. (a) XRD pattern diffraction for Fe_3O_4 in powder (the inset shows the magnetic nanoparticles in colloidal suspension), (b) TEM images of MNPS suspended in cyclohexane and then (c) stabilized with CTAB (for both pictures the insets show the size distribution histogram).

Fig. 2. Electronic spectra for Fe_3O_4@CTAB/PSS films deposited onto the glass surface with different numbers of bilayers. The top inset shows the absorbance vs. number of Fe_3O_4@CTAB/PSS bilayers.

Fig. 3. FTIR spectra of the samples CTAB@Fe_3O_4 (casting), PSS (casting), PSS-CTAB@Fe_3O_4 (casting), and Fe_3O_4@CTAB/PSS LbL 15-bilayer film.

Fig. 4a. AFM topographic of Fe_3O_4@CTAB/PSS 10-bilayer LbL film, using tapping mode on BK7 glass substrate. b) Three-dimensional view by AFM for 2 bilayers (I), 5 bilayers (II) and 10 bilayers (III) LbLFe_3O_4@CTAB/PSS films.

Fig. 5. Cyclic voltammograms using Fe_3O_4@CTAB/PSS LbL film (2 bilayers) as working electrodes in phosphate buffer (BS, 0.1 mol L^{-1}, pH 7.1) in presence of H_2O_2 (500 μmol L^{-1}) with no-purging (dashed line) and purging (continuous line) with N_2 at scan rate of 0.05 V s^{-1}. Inset: Cyclic voltammograms for FTO substrate (in red) and Fe_3O_4@CTAB/PSS LbL film (2 bilayers) (in black) in presence of H_2O_2 (600 μmol L^{-1}) at scan rate of 0.05 V s^{-1}.

Fig. 6. Cyclic voltammograms recorded at 0.05 V s^{-1} in 0.1 M BS (0.1 mol L^{-1}, pH 7.0) for a 2-bilayer Fe_3O_4@CTAB/PSS film in the presence of H_2O_2 at concentrations from 0.1 to 1.8 mmol L^{-1}. Inset: Analytical curve of Fe_3O_4@CTAB/PSS LbL film (2 bilayers) obtained by cyclic voltammetry: intensity of the reduction peak vs. [H_2O_2] at ca. -0.6 V.

Fig. 7. Cyclic voltammograms at different scan rates of (a) 0.005, (b) 0.015, (c) 0.025, (d) 0.050, (e) 0.075, (f) 0.100, (g) 0.150, (h) 0.200, (i) 0.250, (j) 0.300, (k) 0.350, (l) 0.400, (m) 0.450 and (n) 0.500 V s^{-1} for a 2-bilayer LbL film of Fe_3O_4@CTAB/PSS ([Fe_3O_4@CTAB/PSS]$_2$). Inset: linear relationship between reduction peak intensity of the H_2O_2 and square root of the scan rate. Supporting electrolyte: 1 m mol L^{-1} of H_2O_2 in PB solution (0.1 mol L^{-1}, pH 7.1).

Fig. 8. Typical steady state current response curves vs. Ag/AgCl by chronoamperometry of the sensor [Fe_3O_4@CTAB/PSS]$_2$ toward an increasing concentration of hydrogen peroxide.

Inset: analytical plot of the LbL sensor $[Fe_3O_4@CTAB/PSS]_2$ toward H_2O_2 (each point is the average value for 3 different electrodes) ($R^2 = 0.994$). Supporting electrolyte: PB at 0.1 mol L^{-1}, pH 7.1. Applied potential: -0.3 V. Response time: 60 s.

Fig. 9. Current potential curve for a 2-bilayer Fe_3O_4@CTAB/PSS LbL film vs. Ag/AgCl after addition of H_2O_2 and interferents: KCl (670 μmol L^{-1}), NaCl (800 μmol L^{-1}), $MgCl_2.6H_2O$ (300 μmol L^{-1}), $CaCl_2$ (600 μmol L^{-1}), Uric Acid (300 μmol L^{-1}). Supporting electrolyte: PB (0.1 mol L^{-1}, pH 7.1).

Highlights

Fabrication of LbL films of Fe_3O_4@CTAB nanoparticles and PSS.

A non-enzymatic biomimetic system based on Fe_3O_4@CTAB nanoparticles.

The sensor has good response to H_2O_2.

The sensor is comparable with some biosensors based on peroxidase enzyme.

The Fe_3O_4@CTAB/PSS sensor may find applications in environmental industries.

Table 1 Roughness average (R_a) and Root mean square roughness (R_q) values obtained for different amount of bilayers deposited on the glass substrate.

# of bilayers	R_a (nm)	R_q (nm)
2	8.5 ± 1.1	10.6 ± 2.2
5	11.1 ± 1.2	10.7 ± 2.2
10	4.8 ± 0.1	6.0 ± 0.2

Table 1

Table II List of references regarding H_2O_2 detection via amperometric electrochemical methods. Abbreviations: E_{appl}: applied work potential; SCE: saturated calomel electrode; GS–Nafion/Fe3O4–Au-HRP: magnetic nanoparticles coated with HRP and graphene sheets–Nafion; PpPDA@Fe_3O_4-Hb: immobilized hemoglobin (Hb) onto poly(p-phenylenediamine)-ferromagnetic nanoparticles nanocomposite; LbL films based on hemoglobin immobilized on Pt core–shell magnetic nanoparticles; Fe_3O_4–Ag: magnetic submicrospheres (diameter of 400 nm) decorated with Ag nanoparticles; GCE-Fe_3O_4/CS-Hb: hemoglobin immobilized on glassy carbon electrode based on microsphere of chitosan containing magnetic nanoparticles; Fe_2O_3–BMIM-PF6–CP: Carbon paste electrode modified with γ-Fe_2O_3 and 1-butyl-3-methylimidazolium hexafluorophosphate (BMIM-PF6).

Sensor configuration	E_{appl} (V)	Linear up to (μM)	Sensitivity ($nA\mu M^{-1}$)	LOD (μM)	Ref.
Fe3O4@CTAB/PSS	–0.3 vs. Ag/AgCl	1600	16	103	Here
GS–Nafion/Fe3O4–Au-HRP	–0.3 vs. Ag/AgCl	2500	-	12	(Xin et al., 2013) [41]
PpPDA@Fe_3O_4-Hb	–0.4 vs. SCE	400	76	0.21	(Baghayeri et al., 2014) [23]
Hb/Fe_3O_4@Pt	–0.4 vs. SCE	160	1500	0.03	(Yut et al., 2013) [16]
Fe_3O_4–Ag	–0.5 vs. Ag/AgCl	3500	–	1.2	(Liu et al., 2010) [15]
GCE-Fe_3O_4/CS-Hb	–0.15 vs. Ag/AgCl	1800	0.315	4	(Tan et al.,2009) [42]

Fe_2O_3–BMIM-PF6–CP	–0.1 vs. SCE	1500	206.51	0.8	(Baratella et al., 2013) [43]

Figures

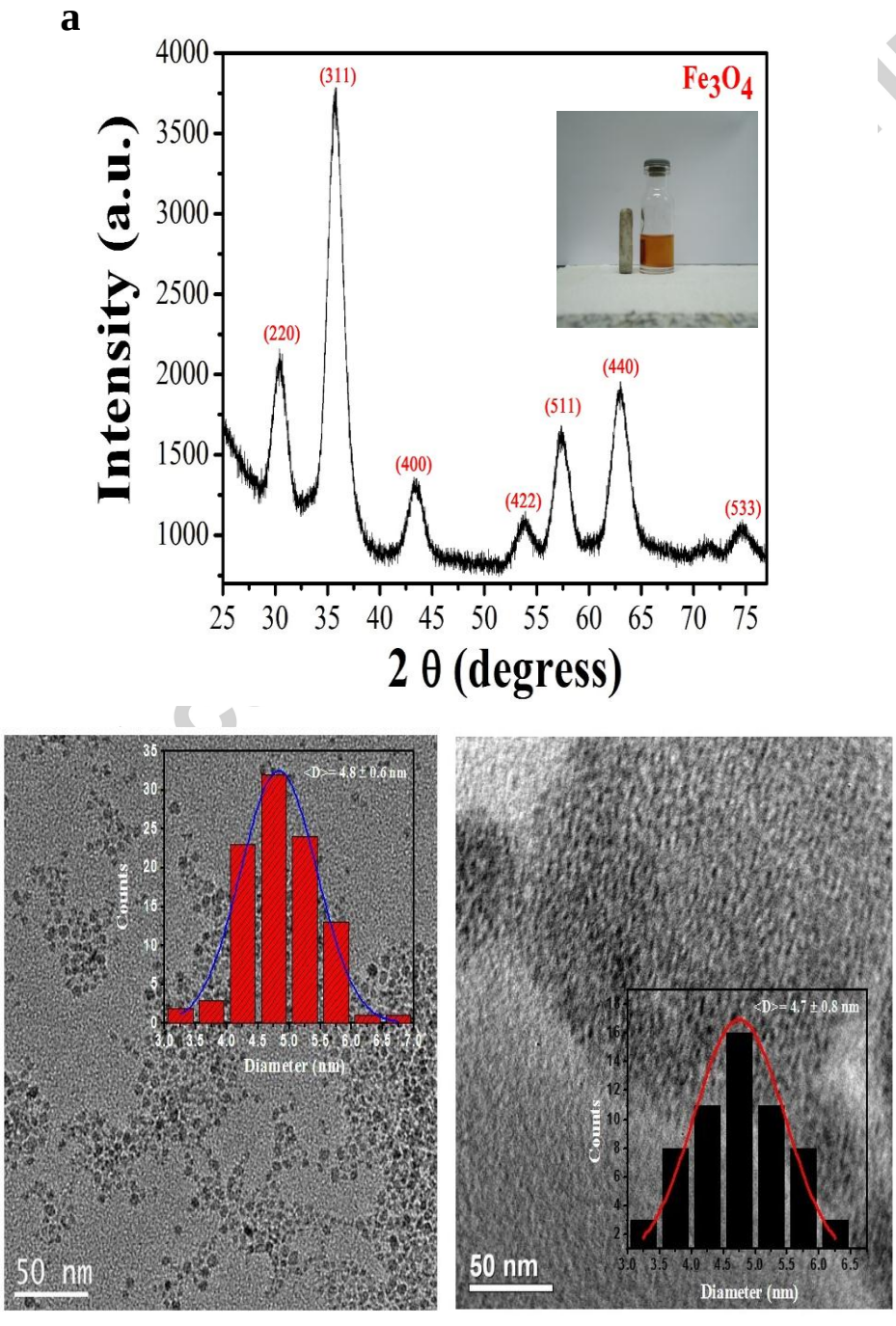

Figure 1

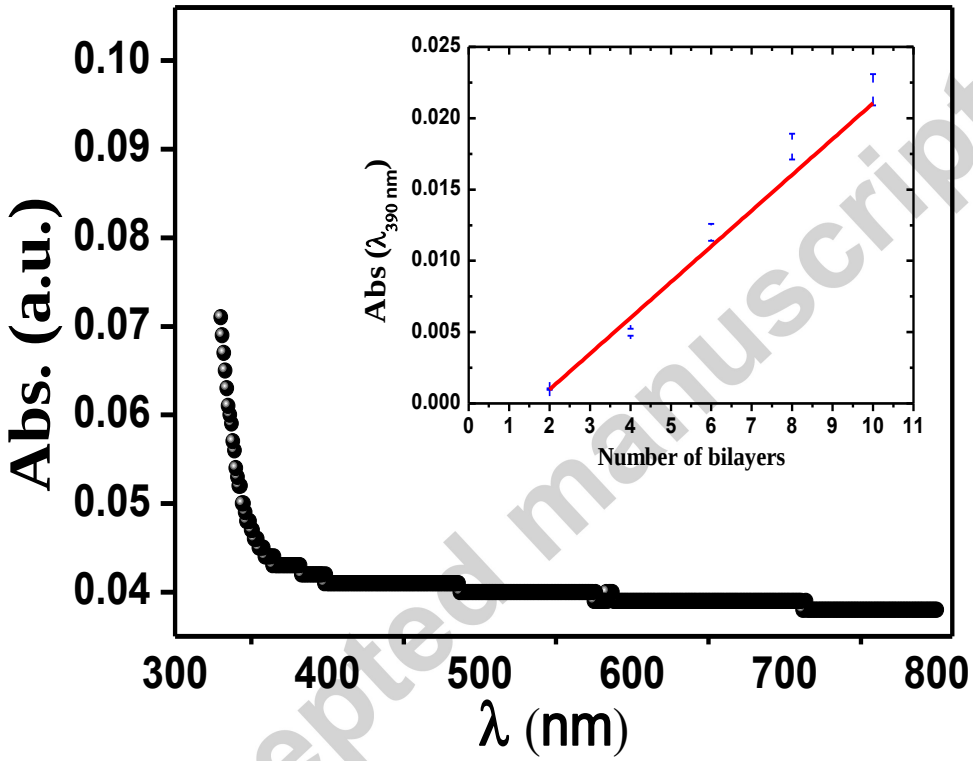

Figure 2

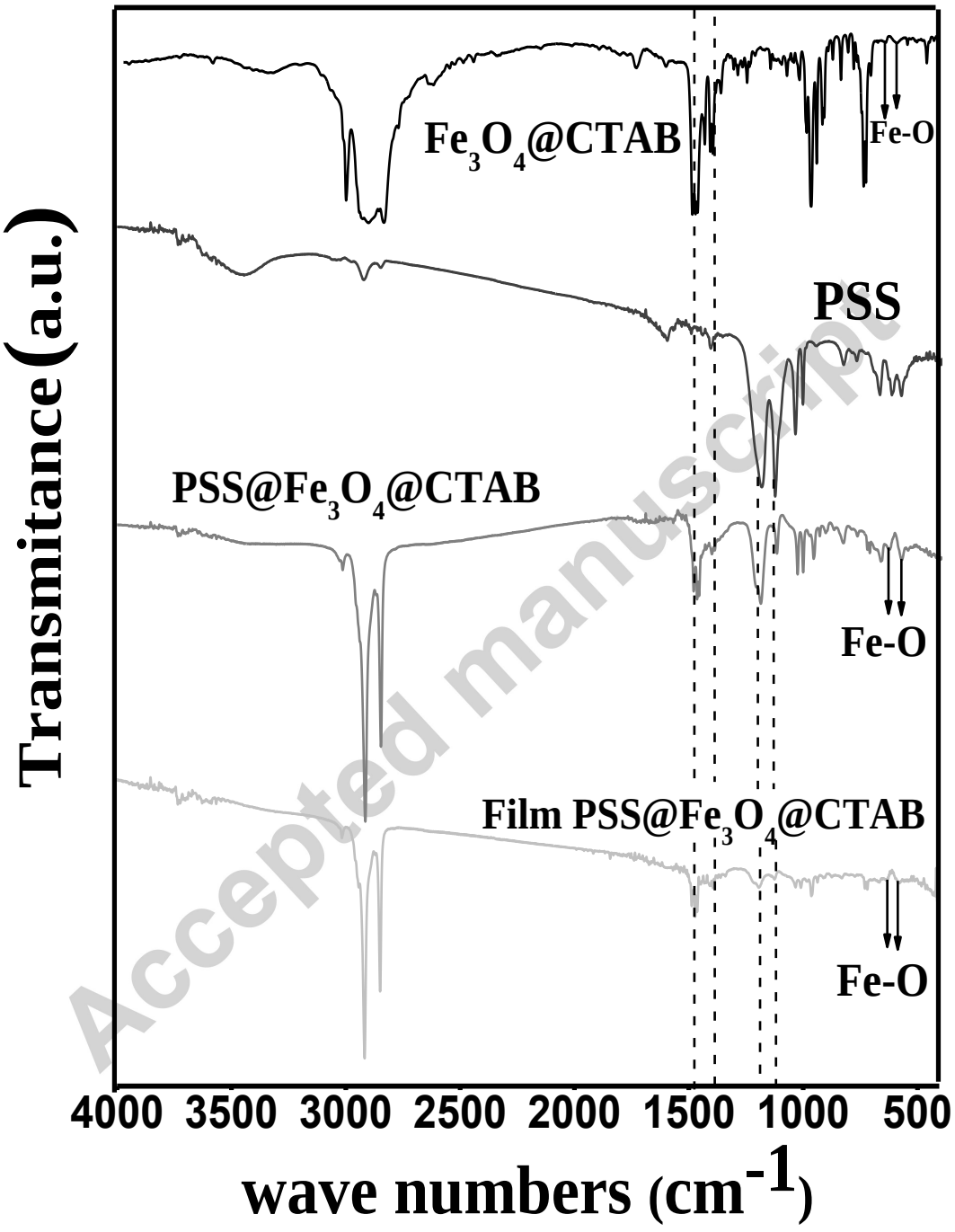

Figure 3

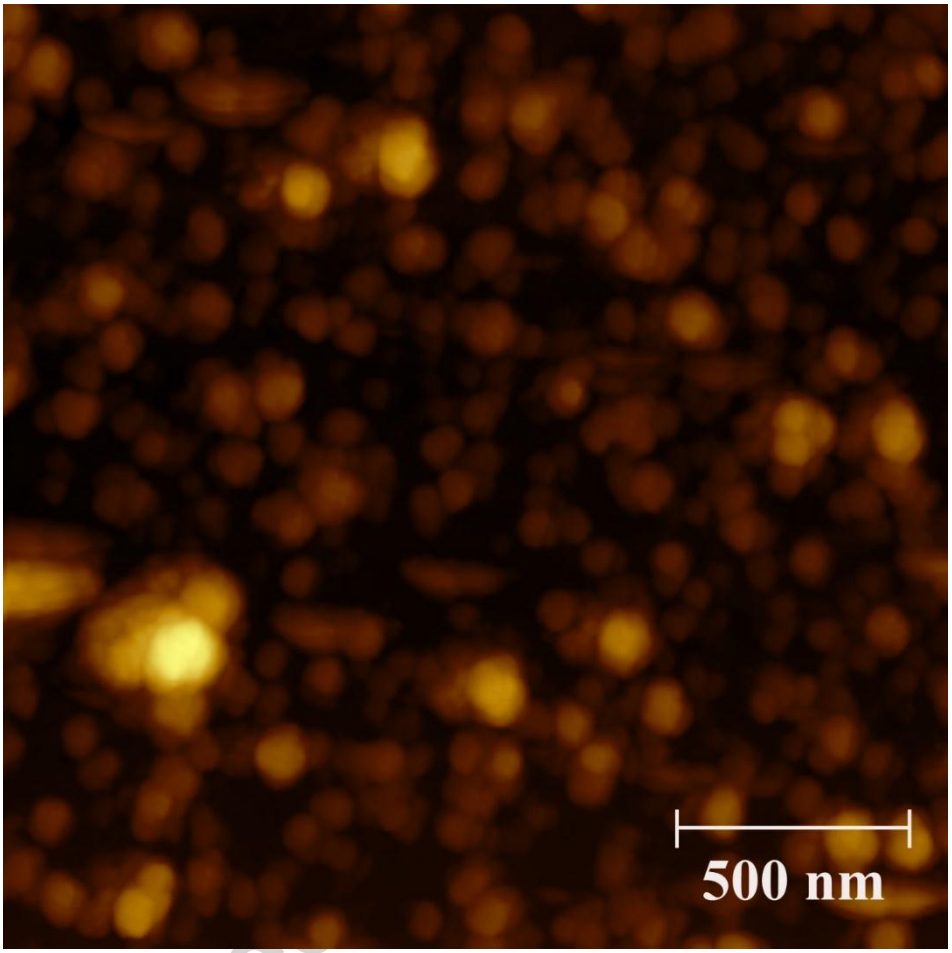

b)

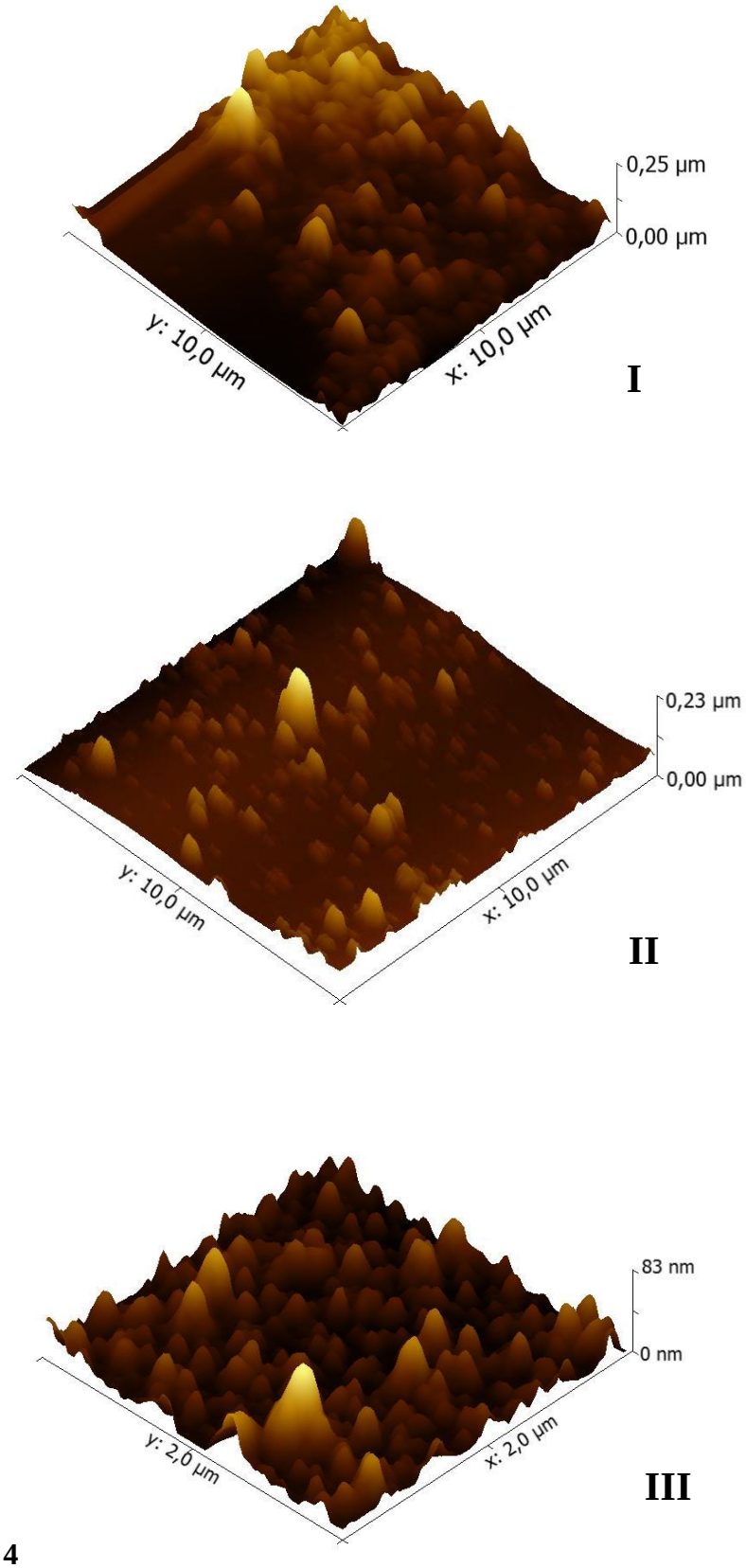

Figura 4

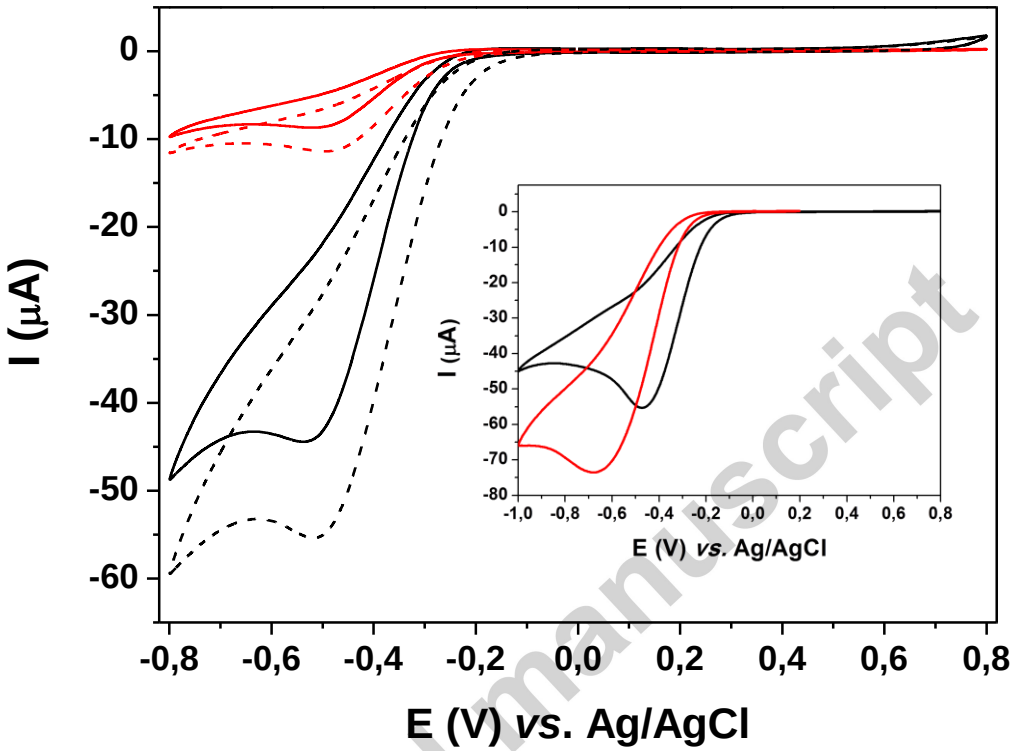

Figure 5

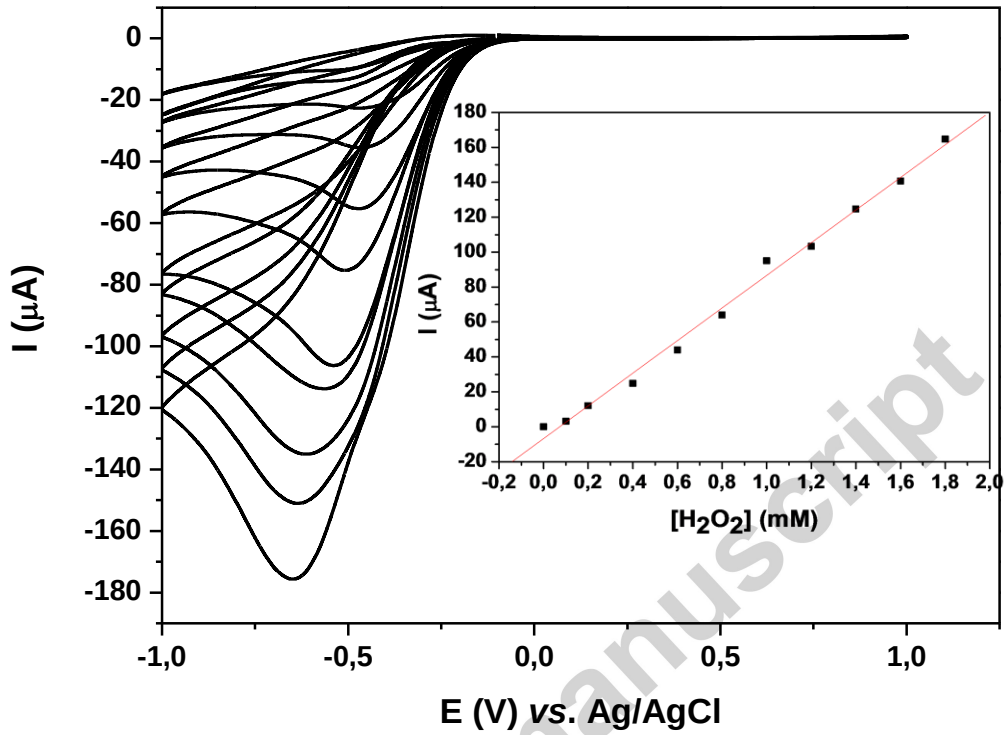

Figure 6

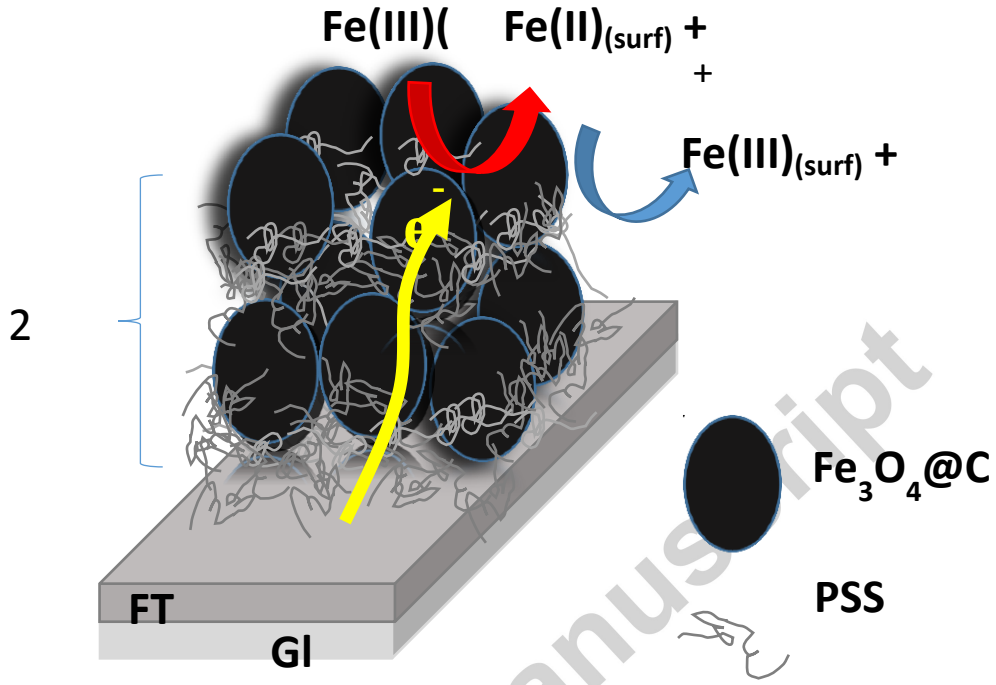

Scheme 1

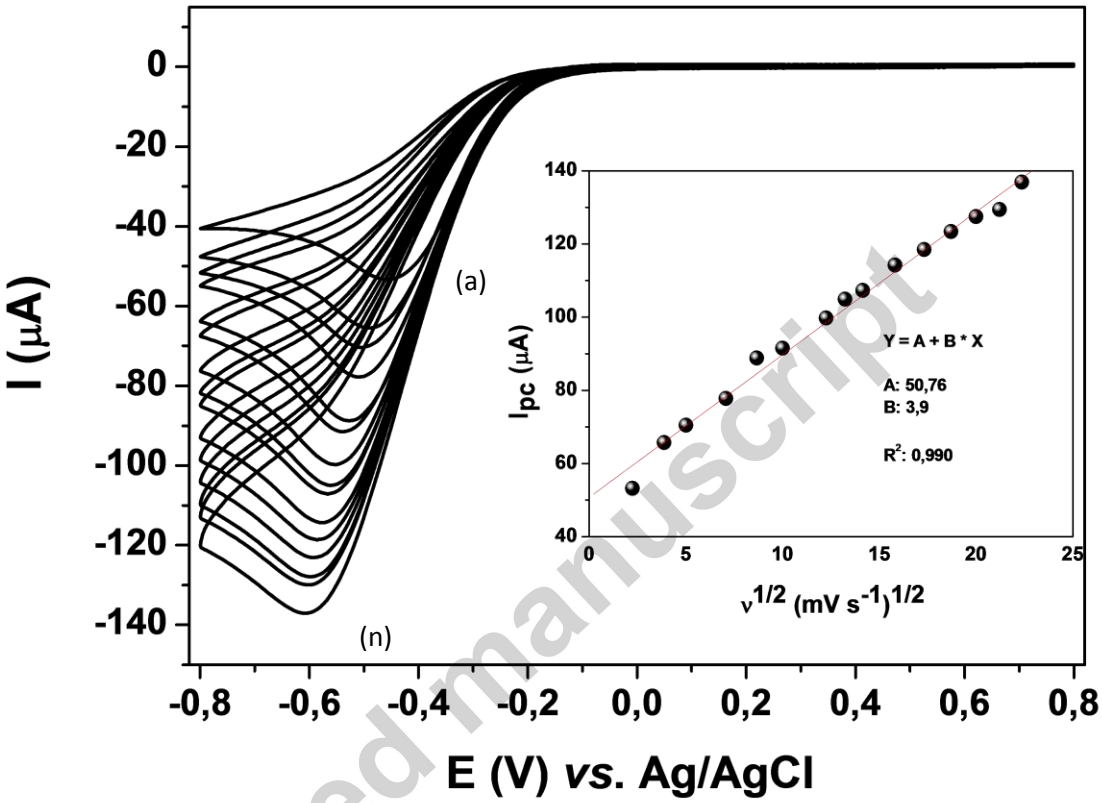

Figure 7

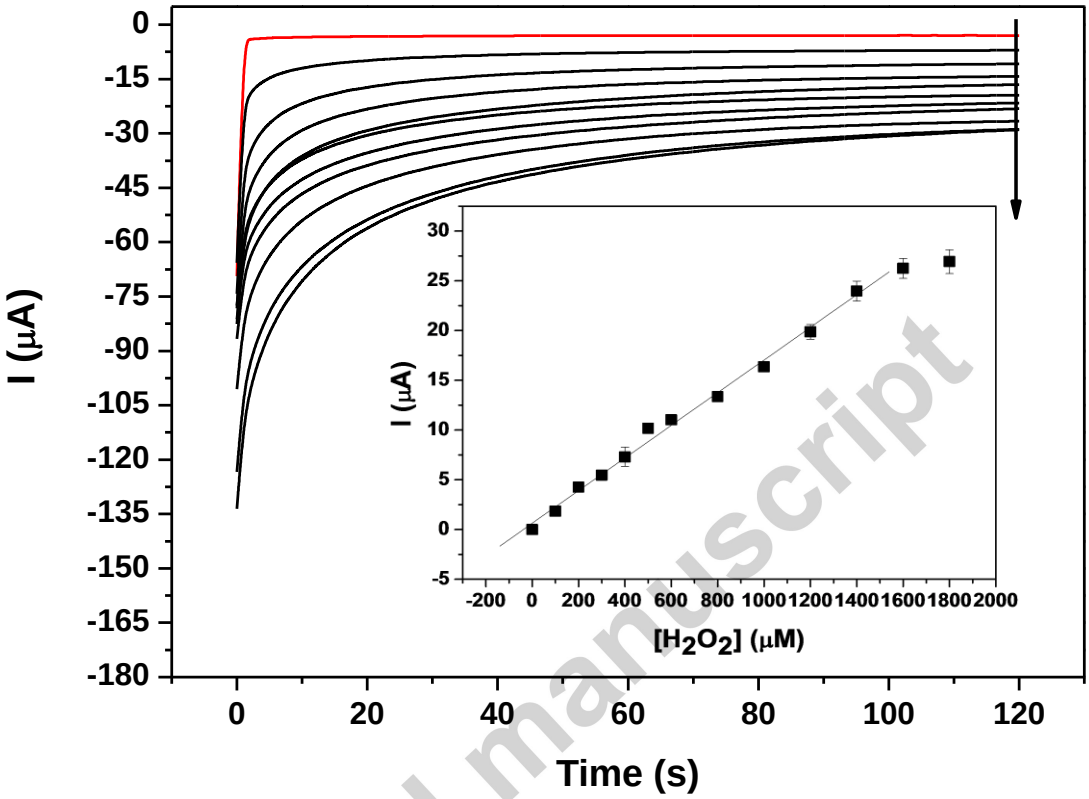

Figure 8

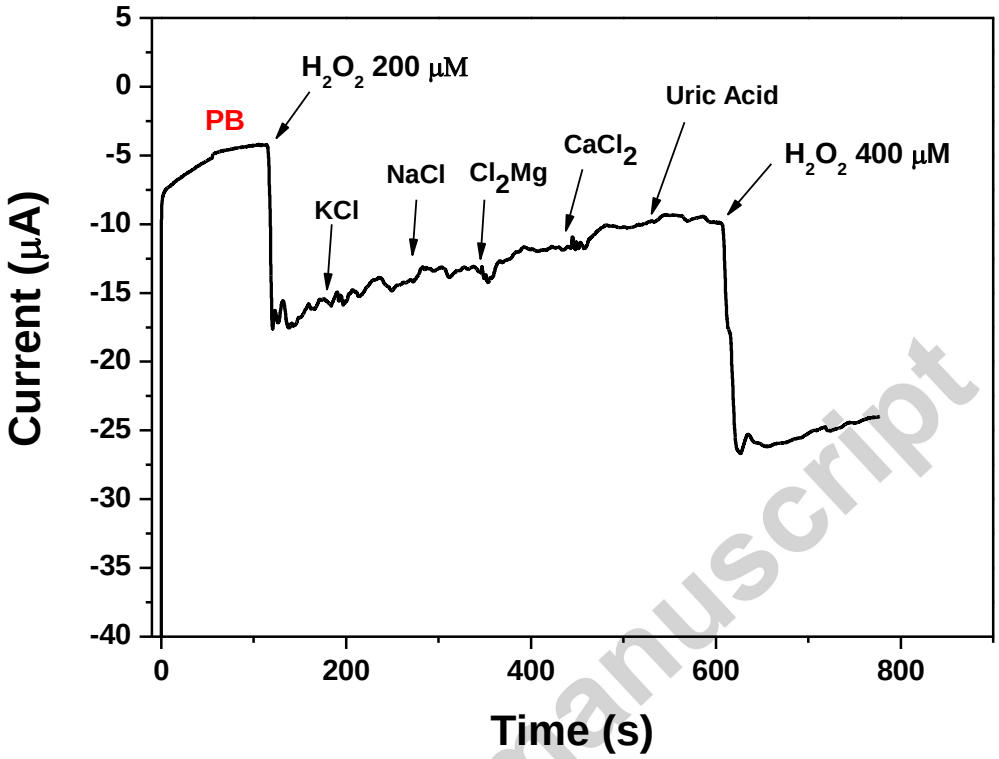

Figure 9